PROBABILISTIC SEISMIC HAZARD ANALYSIS FOR AREQUIPA CITY, PERU

ANÁLISIS DE PELIGRO SÍSMICO PROBABILÍSTICO PARA LA CIUDAD DE AREQUIPA, PERÚ

Carlos Concha[1*], Carlos Gonzales[2], Manuel Monroy[3], Juan Carlos Tarazona[4]

[1]*Geotechnical Engineer, Hatch Ltd, Niagara Falls, Canada*

[2]*Japan Peru Center for Earthquake Engineering Research and Disaster Mitigation, Lima, Peru*

[3]*Senior Principal Geotechnical Engineer, Geosyntec Consultants, Vancouver, Canada*

[4]*Faculty of Civil Engineering, National University of Engineering, Lima, Peru*

Received (Recibido): 04 / 03 / 2025 Publicado (Published): 30 / 12 / 2025

ABSTRACT

Arequipa, located in southern Peru, lies in a region of significant seismic potential known as the Pacific Ring of Fire. This high seismic activity is closely linked to the subduction process, where the Nazca Plate converges beneath the South American Plate at an average rate of 70 mm/year. This study presents an updated and detailed Probabilistic Seismic Hazard Analysis (PSHA) for Arequipa, incorporating a comprehensive seismic catalog that spans historical and instrumental seismicity from 1471 to 2023. In addition to subduction-related sources, this study also considers Quaternary crustal faults. Seismological parameters such as Beta (β) and activity rate (λ) were estimated using the maximum likelihood method, considering catalog completeness assessment.

The analysis includes both subduction zones, modeled with a doubly bounded exponential distribution, and quaternary faults, modeled with a maximum magnitude frequency model. Epistemic uncertainties were addressed through a logic tree framework, incorporating various Ground Motion Models (GMMs) weighted by their relevance. The GMMs used for subduction are based on the latest models available. Site conditions were classified as soils type B (Vs_{30}= 760 m/s).

Seismic disaggregation reveals that earthquakes with magnitudes between Mw 7.5 and 8.0 at distances of 100-150 km contribute most significantly to the seismic hazard for peak ground acceleration (PGA) and spectral accelerations. The primary contributors are intermediate intraslab events, followed by interface sources. Finally, spectral accelerations were calculated for 10%, 5% and 2% probabilities of exceedance in 50 years , yielding PGA values of 0.44 g, 0.58 g, and 0.80 g, respectively. Due to the low slip rates and long recurrence intervals of seismic activity on Quaternary crustal faults, these sources do not contribute significantly to the seismic hazard probabilities of exceedance higher than 2% in 50 years.

Keywords: Probabilistic seismic hazard analysis, ground motion models, peak ground acceleration, spectral accelerations, Arequipa

RESUMEN

Arequipa, ubicada en el sur de Perú, se encuentra en una región de significativo potencial sísmico conocida como el Cinturón de Fuego del Pacífico. Esta alta actividad sísmica está estrechamente relacionada con el proceso de subducción, donde la Placa de Nazca converge bajo la Placa Sudamericana a una tasa promedio de 70 mm/año. Este estudio presenta un Análisis de Peligro Sísmico Probabilístico (PSHA) actualizado y detallado para Arequipa, incorporando un catálogo sísmico integral que abarca la sismicidad histórica e instrumental desde 1471 hasta 2023. Adiocionalmente a las fuentes de subduccion, este estudio tambien considera fallas corticales cuaternarias. Los parámetros sismológicos como Beta (β) y la tasa de actividad (λ) se estimaron utilizando el método de máxima verosimilitud, considerando la evaluación de la completitud del catálogo.

El análisis incluye tanto zonas de subducción, modeladas con una distribución exponencial doblemente acotada, como fallas cuaternarias, modeladas con un modelo de frenquency de magnitud máxima. Las incertidumbres epistémicas se abordaron a través de un marco de árbol lógico, incorporando varias Ecuaciones de Predicción de Movimiento del Suelo (GMMs) ponderadas por su relevancia. Las GMMs utilizadas para la subducción se basan en los últimos modelos disponibles. Las condiciones del sitio se clasificaron como suelos tipo B (Vs_{30}= 760 m/s).

La desagregación sísmica revela que los terremotos con magnitudes entre Mw 7.5 y 8.0 a distancias de 100-150 km contribuyen más significativamente al peligro sísmico para la aceleración máxima del suelo y aceleraciones espectrales. Los principales

[1] * Carlos Concha:
E-mail: jose.concha.t@uni.pe

contribuyentes son eventos intraplaca intermedios, seguidos por fuentes de interfaz. Se calcularon valores de aceleraciones espectrales para 2%, 5% and 10% de probabilid de excedencia en 50 años, obteniendo PGAs de 0.44g, 0.58g y 0.80g, respectivamente. Debido a la baja tasa de desliazamiento y a intervalos de recurrencia sismica largos de las fallas corticales quaternarias, estas fuentes no contribuyen al peligro sismico probabilistico para probabilidades de excedencia mayores de 2% en 50 años.

Palabras Clave: Análisis de Peligro Sísmico Probabilístico, ecuaciones de predicción del movimiento, aceleración pico del suelo, aceleraciones espectrales, Arequipa

1. INTRODUCTION

Probabilistic Seismic Hazard Analysis (PSHA) is an approach used to predict the probability of different levels of ground shaking at a specific site comprising variability in earthquake size, location and frequency. This methodology considers seismological, geological and geotechnical data to provide a comprehensive understanding of seismic hazard. For Arequipa, a city placed in a highly seismically active region and experience continuous growth, un update of the PSHA is crucial to determine the dominant earthquake scenarios to contribute to local hazard levels with the objective of supporting urban planning and risk management strategies.

Many studies developed seismic hazard analysis for southern Peru. Monroy et al. [1] conducted a probabilistic seismic hazard analysis (PSHA) using a doubly truncated exponential model and the Youngs & Coppersmith model [2] to estimate seismic design parameters for Lima, Arequipa, Huancayo, and Puno, focusing on a 10% probability of exceedance in 50 years (475-year return period). In Arequipa, the disaggregation analysis revealed that earthquakes with magnitudes between M7.5 and M8.0, occurring at source-to-site distances of 125–150 km, contribute most to seismic hazard. Aguilar & Tarazona [3] developed a PSHA for Peru considering 34 seismic sources (7 inteface, 15 intraslab and 12 crustal) modeled with exponentially truncated Gutenberg-Richter model. Maximum magnitudes used for the interface sources ranged from M8.7 to M9.0, and from M7.7 to 8.0 for intraslab sources. The Peak Ground Acceleration (PGA) for Arequipa city was estimated to range from 0.43 g to 0.46 g for 10% probability of exceedance, and from 0.80 g to 0.84 g for 2% probability of exceedance.

All prior PSHA's were developed using similar methodologies and approaches. However, this study incorporates more up-to-date Ground Motion Models (GMMs) and models subduction zones using a doubly bounded exponential distribution with updated maximum magnitudes based on recent research specific to the South America subduction zone, such as Muldashev & Sobolev [4], Carena [5] and Tarazona et al. [6]. Additionally, it accounts for quaternary faults, which are modeled using the maximum magnitude characteristic approach.

2. SEISMIC CATALOG FOR SOUTHERN PERU

For this research, seismic event information was gathered based on both historical and instrumental seismicity. Historical seismicity was compiled from various sources, including Silgado [7], Dorbath et al. [8], Tavera [9], and Tavera et al. [10]. Instrumental seismic data were collected from seven seismic catalogs, covering an extensive geographical region from 76° to 67° west longitude and from 12° to 21° south latitude. This area extends approximately 500 kilometers from the center of the city of Arequipa. The instrumental seismic data includes events up to December 31, 2023, encompassing subduction events with magnitudes of Mw 4.0 and above. These records were obtained from seismic catalogs provided by the Instituto Geofísico del Perú (IGP)[11], United States Geological Survey (USGS)/Advanced National Seismic System (ANSS)[12], International Seismological Centre (ISC) – Global Earthquake Model Foundation (GEM), International Seismological Centre (ISC) revised[13], Global Centroid Moment Tensor (CMT)[14], National Earthquake Information (NEI)[15], and National Oceanic and Atmospheric Administration (NOAA) – Global Significant Earthquake Database[16].

2.1. Duplicate Event Removal

Given that the compiled catalog integrates data from seven distinct sources, it is common for the same seismic event to be reported by multiple agencies, resulting in duplicate entries. The initial dataset, obtained directly from the respective agencies, included a total of 43,779 seismic events. However, some catalogs—such as the ISC—contained both bulletin and reviewed versions, where even within a single source, the same event could be listed multiple times with differing magnitude scales. To address this, the first step involved removing internal duplicates within each catalog. This was done by prioritizing the moment magnitude scale (Mw), followed by surface-wave magnitude (Ms), body-wave magnitude (mb), local magnitude (ML), and finally unknown magnitude types (Unk). Through this internal filtering process, the number of events was reduced to 26,653.

Subsequently, inter-catalog duplicates were addressed by grouping seismic events that occurred within a temporal window of 60 seconds and had epicenters located within a 70 km radius of each other. These thresholds were established based on an exploratory analysis of the catalog data, which showed that, for events clearly representing the same earthquake but reported by different agencies, the average differences in origin time and epicentral location were approximately 60 seconds and 70 km, respectively. Each group was assumed to represent a single seismic event detected by multiple agencies. Within each group, one representative entry per catalog was retained to maintain traceability. A selection hierarchy was then applied to retain only the most reliable record. The CMT catalog was assigned the highest priority due to its comprehensive and consistent seismic data. The IGP catalog was ranked second, reflecting its dense seismic monitoring network in Peru. The NOAA and ISC-GEM catalogs were given third-level priority, while the remaining sources were treated equally. Based on this hierarchy and the magnitude scale preference, a single representative record was selected from each group, and the remaining entries were removed. After completing this deduplication process, the final catalog contained 15,063 unique seismic events.

2.2. Magnitude Scale Homogenization

In seismological practice, the magnitude of seismic events is represented through various scales, with Moment Magnitude (Mw) being the preferred scale in contemporary seismic engineering due to its non-saturating nature and correlation with physical parameters, like fault displacement and energy release. Other scales, such as Surface-Wave Magnitude (Ms) and Body-Wave Magnitude (mb), rely on empirical relationships derived from seismometer-recorded wave amplitudes by McGuire [17]. This study establishes a hierarchy for representing seismic events, prioritizing Mw first, followed by Ms, mb, Local Magnitude (mL), and Unknown Magnitude (Unk) scales. To standardize measurements across all seismic events in the compiled catalog, the Mw scale, proposed by Hanks and Kanamori [18], is selected for its ability to remain unsaturated during large magnitude events and its direct link to the energy released at the seismic source, derived from the scalar seismic moment (Mo). Most of the current GMMs are based on Mw scale, reinforcing its selection as the standard measure. The relationship proposed by Kadirioglu et al. [19] for ML scale was employed for magnitudes in the range $3.3 \leq ML \leq 6.6$. For the mb and Ms scales, the expressions provided by the International Seismological Center (ISC) as defined by Scordilis [20] are used. Events with an unknown magnitude were removed. Despite the standardization, the catalog reports seismic events on the Mw scale, and henceforth, this report will use the notation "M" to refer to seismic magnitude.

2.3. Declustering of Dependent Events

The seismic hazard analysis in this study follows a Poisson distribution, requiring the exclusion of dependent seismic events to ensure a dataset dominated by independent occurrences within specific spatial and temporal intervals. This approach safeguards the randomness, independence, and consistent frequency of the final catalog. The declustering process utilized deterministic methods with circular windows, where temporal and spatial dimensions were calibrated based on the magnitude of the mainshock. Both foreshocks and aftershocks were treated equitably, with a minimum one-unit magnitude difference enforced between mainshocks and their dependent events.

Among the declustering methodologies applied, Stiphout et al. [21] is the most restrictive in terms of event removal, discarding approximately 14,000 dependent events, followed closely by Gardner and Knopoff [22], which eliminated ~13,000 events. In contrast, Maeda [23] and Uhrhammer [24] demonstrated more limited resctriction, removing ~12,800 and ~9,200 events, respectively. These results were evaluated through cumulative event series, with Stiphout et al. [21] and Gardner and Knopoff [25] exhibiting linear trends with consistent slopes since 1960, free from significant anomalies. Given their aggressiveness and efficiency, these two methods were selected as the primary approaches for this study. To account for methodological variability and reduce uncertainty in catalog processing, equal weighting (0.50) was assigned to the results of each method, with the declustered catalogs referred to as Catalog 1 and Catalog 2, respectively.

2.4. Seismic Catalog Completeness Analysis

It is observed that the refined seismic catalog indicates that the magnitudes of the recorded earthquakes are not completely available for the same observation periods, especially concerning low-magnitude earthquakes. To use this information more consistently and reliably, earthquakes were grouped by their magnitudes in 0.5 intervals to evaluate the completeness of the catalog according to the method established by Stepp [26]. Earthquakes with magnitudes between M4.5 and M5.0 have been complete since 1984; M5.0 to M5.4 since 1975; M5.5 to M5.9 since 1960; M6.0 to M6.4 since 1932; M6.5 to M7.4 since 1903; M7.5 to M7.9 since 1543; and those greater than M8.0 since 1471 (**Fig. 1**).

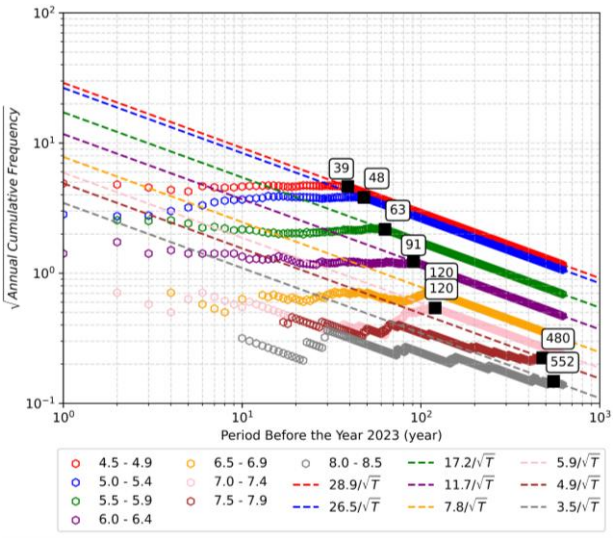

Fig. 1. Completeness Analysis of Catalog 1 (Stepp Method, 1972) – Seismic Catalog of Southern Peru of this Study

A comparative assessment of the completeness periods between the seismic catalog developed in this study and that of Aguilar & Tarazona [3] demonstrates a high level of consistency, despite the broader geographic scope of the latter. While Aguilar's catalog encompasses the entire Peruvian territory, the present study focuses exclusively on southern Peru, yet achieves comparable completeness intervals across various magnitude ranges. For events with magnitudes below Mw 5.9, the current catalog yields a completeness period of 63 years, which is slightly longer than the 62 years reported by Aguilar. In the Mw 6.0 – 7.4 range, the completeness duration is 120 years in this study, closely aligning with the 122 years identified in the national catalog. Notably, for large-magnitude events (Mw ≥ 7.5), the present catalog attains a completeness period of 552 years, surpassing the 509 years reported in Aguilar's study. These results underscore the robustness and reliability of the southern Peru catalog used in this study, affirming its suitability for regional seismic hazard assessments.

3. CHARACTERIZATION OF SEISMIC SOURCES IN AREQUIPA REGION

Once the declustered seismic catalog is obtained, it is grouped based on similar characteristics, such as recurrence rate, seismo-tectonic origin, and geometry, among others.

3.1. Tectonic Categorization of Seismic Events

For the classification of seismic events within the declustered catalog according to their tectonic regime, interface earthquakes are considered first. These are seismic events with depths ranging from 0 to 60 km, occurring in the coupling zone (contact area) between the Nazca Plate and the South American Plate. These events typically originate from reverse faulting mechanisms due to compressional forces between the plates. Interface earthquakes, characterized by significant and relatively shallow vertical displacement of the ocean floor, have a high potential to generate tsunamis, as demonstrated by 1960 Valdivia, Chile [27] and 2001 Arequipa, Peru [28]. Intraslab earthquakes, on the other hand, occur within the Nazca Plate due to the subduction process, with depths exceeding 60 km and extending to 660 km or 700 km, where the seismic behavior transitions from brittle to ductile. Crustal earthquakes occur within the continental plate, at depths less than 60 km or above the Mohorovicic discontinuity (Moho), defined using the LITHO 1.0 Crust model by Pasyanos et al. [29]. Due to uncertainty, the crustal earthquake boundary is set 20 km below Moho. Additionally, outer-rise seismicity refers to earthquakes that take place on the Nazca Plate in the region just preceding the oceanic trench. These are generally shallow events with magnitudes below 7.0, possessing little potential to generate tsunamis.

To account for the inherent uncertainty in the calculation of the hypocenter for each seismic event, error margins will be applied for classification. The boundary for interface events will be set 20 km above and below the coupling zone, while for intraslab events, the boundary will be 20 km above and 60 km below the plate. These criteria are derived from the study by Pagani et al. [30]. Events that do not meet these established criteria will be categorized as "unclassified" earthquakes. It is important to note that both "unclassified" and "outer-rise" events are excluded from contributing to the formation of seismic sources. This approach ensures a coherent and consistent grouping of seismic events into specific tectonic categories.

3.2. Geometry of Subduction Zone Sources

Subduction zone sources were defined considering several factors, including similarity in seismic parameters across adjacent areas, the distribution of historical earthquakes, geological structures, and geometric features of the subduction slab, such as dip angle and convergence velocity. A preliminary segmentation of the region was conducted using square subareas of 200 km per side. This initial grouping was based on the spatial distribution of magnitude-frequency, with Beta (β) values calculated to assess their variation throughout the subduction zone. The magnitude-frequency distribution follows the Gutenberg-Richter relationship [31]:

$$log_{10}N(M \geq m) = a - bm$$

Where N(M≥m) represents the number of earthquakes per year with magnitudes greater than or equal to m, and the parameter a reflects the

seismic activity rate. In particular, the total number of earthquakes with M ≥ 0 is given by N(M≥0) = 10^a. However, this formulation is not directly applicable in practical settings, as it is unbounded and may include physically unrealistic magnitudes. To address this, a truncated exponential distribution [32] is used:

$$f_M(m) = \frac{\beta e^{[-\beta(m-m_{min})]}}{1 - e^{[-\beta(m_{max}-m_{min})]}}, m_{min} \leq m \leq m_{max}$$

Where Beta β = ln(10)b, and m_{min} and m_{max} define the minimum and maximum considered magnitudes.

To define the boundary of the subduction sources, multiple criteria were considered, including seismicity depth, Beta value variations, tectonic segmentation, historical seismicity, and convergence rates. During the preliminary segmentation, regions exhibiting similar Beta values were grouped to delineate the final seismic sources. The analysis yielded Beta values for interface sources ranging from 1.9 to 2.3 in Catalogue 1 and from 2.0 to 2.4 in Catalogue 2. For intraslab sources, the Beta values ranged from 1.7 to 2.6 in Catalogue 1 and from 2.1 to 2.8 in Catalogue 2. These results are broadly consistent with those reported by Monroy et al. [1], who documented Beta values between 1.9 and 2.4 for interface sources and between 2.1 and 2.7 for intraslab sources. Notably, intraslab sources in Catalogue 1 display slightly lower Beta values compared to Monroy's findings.

Based on the depth distribution, the intraslab zone was segmented into two intervals: 60–140 km and 140–220 km. As a result, nine subduction sources were identified: three interface sources (F1, F2, and F3), three intermediate-depth intraslab sources (F4, F5, and F6), and three deep intraslab sources (F7, F8, and F9). The Nazca Ridge defines the boundary between sources F1 and F2, while the Iquique Ridge separates F2 and F3 (**Fig. 2**). The interface sources were further constrained using the rupture areas and lengths associated with significant historical earthquakes (1942, M 8.2; 1868, M 8.8–9.2; and 1877, M 8.0–8.8). Intraslab sources, in turn, were delineated based on depth intervals and spatial variations in Beta values. An additional criterion considered was the convergence rate of the Nazca Plate, which moves eastward at approximately 69 mm/year in the region of source F1, and at about 73 mm/year in the regions of sources F2 and F3 [33]. The depth of the subduction contact surface was based on the USGS Slab 2.0 model by Hayes et al. [34].

3.3. Seismic Parameters for Probabilistic Seismic Hazard Analysis

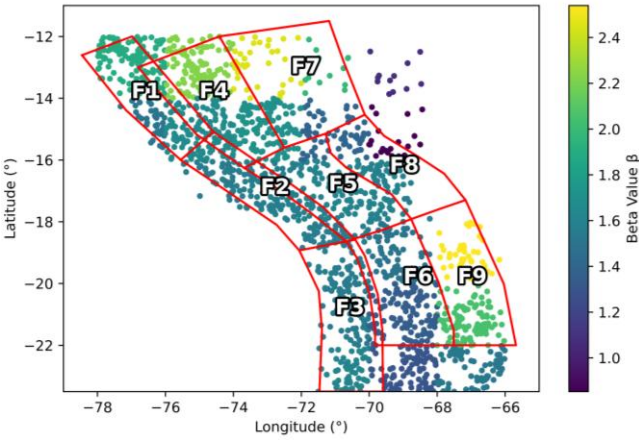

Fig. 2. Variation of the Beta Value in Subduction Sources (Catalog 1)

After defining the boundaries of the area sources using a doubly truncated exponential Gutenberg-Richter model, the next step involves calculating the seismic parameters that characterize each source. These parameters include the Beta value (β), the annual rate of earthquakes greater than or equal to a minimum magnitude λ(M ≥ Mmin), and the maximum magnitude (Mwmax), as summarized in **Table I**. In this study, the maximum likelihood method developed by Weichert [35] was selected to estimate the β and λ(M ≥ Mmin) parameters. This method is particularly suitable for seismic catalogs that include events with different observation periods, as it accounts for catalog incompleteness and aligns well with the assumptions of a Poissonian recurrence model (**Fig. 3**)

The determination of the maximum magnitude of a seismic source can be made through the observation of the highest recorded magnitude, statistical methods, or scaling relationships. However, relying on the maximum observed value in an instrumental catalog has its drawbacks, such as the short observation period compared to the geological age of a fault. Additionally, historical catalogs lack precise magnitudes, creating considerable uncertainty in defining the maximum magnitude of a seismic source. In interface subduction zones, earthquakes with magnitudes greater than Mw 8.5 can occur, but uncertainty remains regarding the factors determining the maximum size of these events. Previous studies suggest that factors, such as the configuration of the subducting plate, the roughness of the plate interface, the deformation states of the involved plates, the thickness of sediments in oceanic trenches, and the subduction velocity, influence this phenomenon. Muldashev & Sobolev [36] stated that low-angle subduction and the presence of coarse sediments in the subduction trench are necessary conditions for generating large-magnitude

earthquakes, which are crucial parameters for determining the maximum magnitude of subduction earthquakes. They also suggest that in the subduction zone of southern Peru and northern Chile, events exceeding magnitude Mw 8.8 can occur. Carena [37] lists historical interface subductionearthquakes greater than Mw 7.7 along the South American trench, with the 1868 earthquake being the largest (Mw 8.8–9.2). Tarazona et al. [38] estimates the maximum magnitude in the Peru subduction zone using the Kijko method [39], Bayesian methods, and scaling relationships, indicating that the interface subduction source in southern Peru, referred to as F-5a in their study (equivalent to sources F1 and F2 in this research), would have a maximum magnitude of M 8.9 (Kijko method) and M 9.0 (Bayesian method). For the intraslab subduction zone, the seismic catalog in this study shows observed maximum magnitudes of M 7.6 to M 7.8. Tarazona et al. [38] assigns maximum magnitudes of M 7.8 to M 8.0 to this region of southern Peru. Kausel and Campos [40] note that the December 9, 1950 earthquake, with a magnitude of M 8.0 and a depth of 100 km, is the only one reported in the Chile subduction zone.

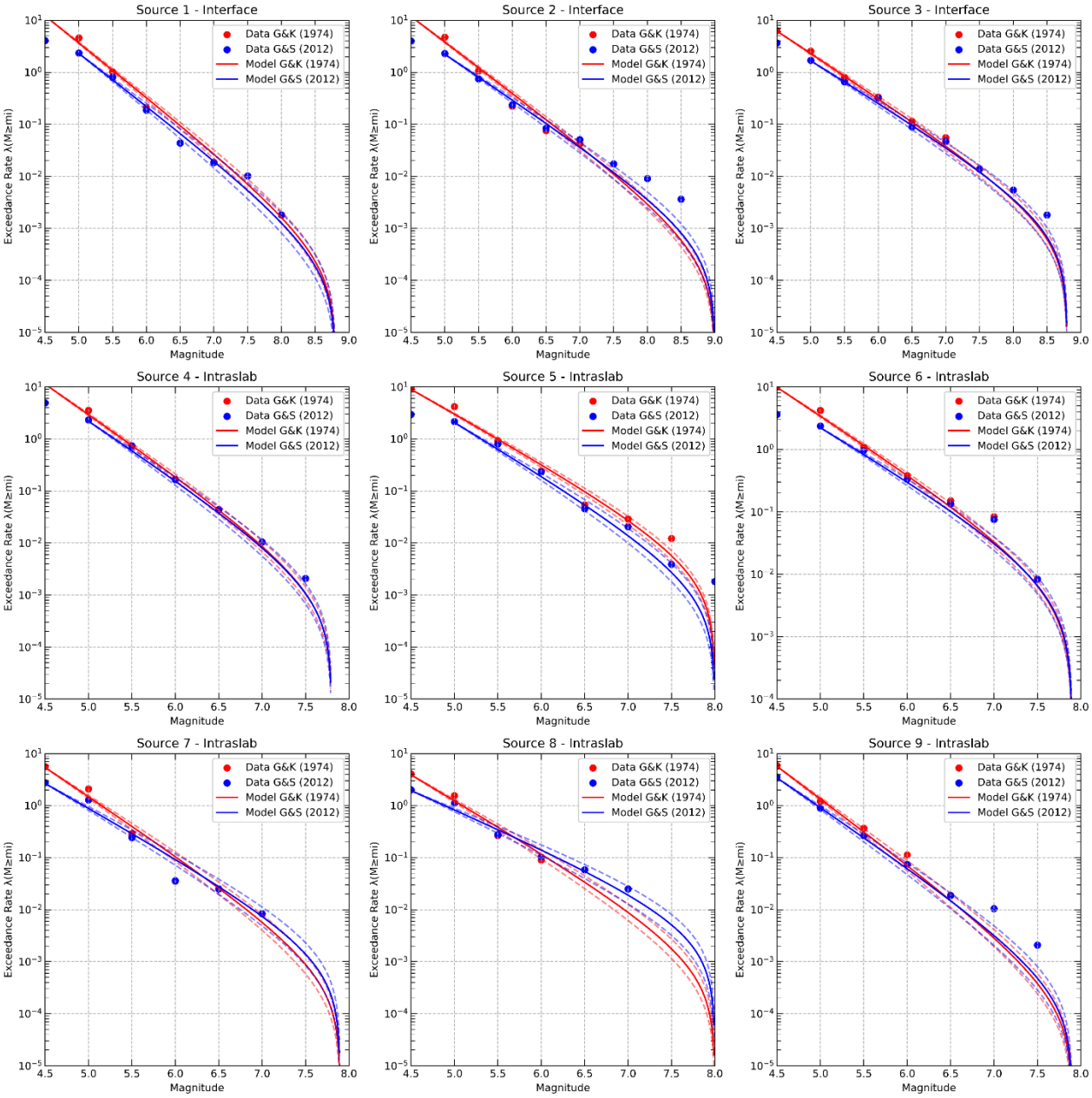

Fig. 3. Seismic Recurrence Distribution with Maximum and Minimum Beta Values – Interface and Intraslab Sources. Red Points and lines Catalog 1 | Blue Points and Lines: Catalog 2

TABLE I
Seismic Parameters for Truncated Exponential Model Across All Area-type Seismic Sources

Seismic Source	Mmin	$\lambda(M \geq M_{min})$	$\Delta\lambda(M \geq M_{min})$	β	Δβ	Mw_{max}
S1-Interface	5.0/4.5	2.350/12.315	0.202/0.509	2.310/2.384	0.147/0.077	8.8±0.2
S2-Interface	5.0/4.5	2.255/11.914	0.192/0.497	2.000/2.247	0.116/0.070	9.0±0.2
S3-Interface	5.0/4.5	1.697/6.277	0.164/0.353	1.859/1.972	0.127/0.078	8.8±0.2
S4-Intraslab	5.0/4.5	2.325/11.720	0.205/0.502	2.539/2.648	0.179/0.095	7.8±0.3
S5-Intraslab	5.0/4.5	2.168/9.281	0.195/0.436	2.301/2.154	0.163/0.075	8.0±0.3
S6-Intraslab	5.0/4.5	2.350/10.212	0.196/0.456	1.908/2.087	0.125/0.072	7.9±0.3
S7-Intraslab	4.5/4.5	2.746/5.579	0.247/0.346	2.159/2.548	0.167/0.139	7.9±0.3
S8-Intraslab	4.5/4.5	2.001/4.028	0.203/0.291	1.681/2.266	0.155/0.142	8.0±0.3
S9-Intraslab	4.5/4.5	3.525/5.867	0.285/0.358	2.598/2.846	0.172/0.150	7.9±0.3
S10-Crustal	4.5/4.5	2.120/6.845	0.214/0.384	2.068/2.646	0.194/0.131	7.5±0.1

3.4. Active Geological Faults

The absence of paleoseismic studies and individualized monitoring has left most geological faults lacking sufficient data to define specific seismic parameters. As a result, crustal seismic activity is represented by a combination of the seismic catalog and geological data from major faults. Using the seismic catalog, a crustal seismogenic source is modeled with a doubly truncated exponential distribution, considering earthquakes within a 300 km radius of Arequipa (**Fig. 4**). Faults characterized by slip rates are represented using a Maximum Magnitude characteristic model.

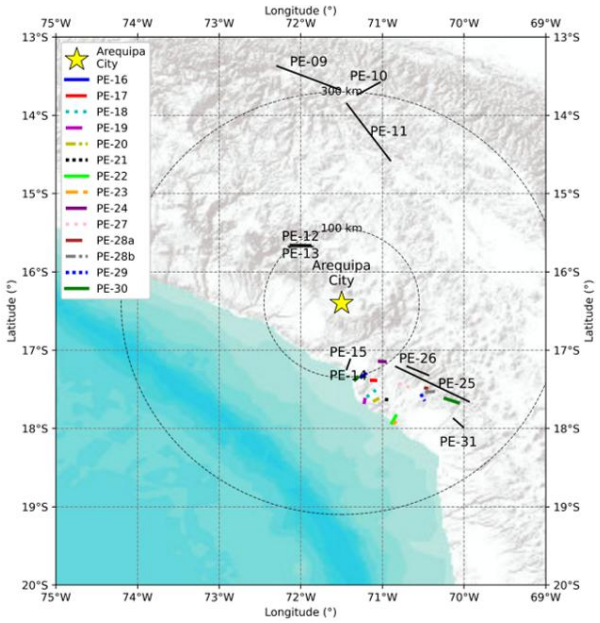

Fig. 4. Active Faults Identified by Machare et al. (2003) considered in this Study

Despite Benavente et al. [41] identifying 81 active faults in their study of the neotectonics and seismic hazard in the Arequipa region, these faults have not been characterized with recurrence intervals. As a result, they are excluded from the probabilistic seismic hazard analysis. Only the faults identified by Machare et al. [42] will be considered and modeled

based on the Maximum Magnitude Earthquake philosophy (**Table II**). Machare et al. [42] conducted a study of active Quaternary faults in Peru as part of the international lithosphere program "World Map of Major Active Faults," funded by the USGS. This study provides data on the location, recent displacement or activity times, and activity rates of major earthquake-related features, including faults and fault-related folds. For the seismic hazard analysis, only active faults within a 300 km radius of Arequipa are considered.

TABLE II
Active Faults within a 300 km Radius of Arequipa City

Fault	Code	Strike/Dip	Length (km)	Estimated Slip Rate (mm/year) (Weight 0.2-0.6-0.2)	Magnitude (Mw) (Min.-Mean-Max.)
Cuzco (N)	PE-09	N63°W/60°	97.4	0.01-0.2-1.0	7.4±0.3
Ocongate (N)	PE-10	N88°E/75°	34.3	0.01-0.2-1.0	6.9±0.3
Vilcanota River (N)	PE-11	N35°W/65°	93.7	0.001-0.01-0.1	7.4±0.3
Trigal (N)	PE-12	N89°E/75°	20.4	0.01-0.2-1.0	6.6±0.3
Solarpampa (N)	PE-13	N90°E/75°	14.4	0.01-0.2-1.0	6.4±0.3
Machado Chico (N)	PE-14	N21°E/60°	16.9	0.001-0.01-0.1	6.5±0.3
Pampa Huanocollo	PE-15	N18°E/40°	12.3	0.001-0.01-0.1	6.3±0.3
Cerro Cordilleras	PE-16	N67E°/50°	19.1	0.001-0.02-0.1	6.6±0.3
Unknown Fault	PE-17	N81°W/50°	10.4	0.001-0.01-0.1	6.3±0.3
Chololo	PE-18	N54°E/50°	16.7	0.001-0.01-0.1	6.5±0.3
Cerro Loreto	PE-19	N11°E/60°	9.2	0.003-0.02-0.1	6.2±0.3
Cerro Chaspaya	PE-20	N61°E/50°	10.2	0.003-0.02-0.1	6.2±0.3
Cerro Chascoso	PE-21	N4°E/70°	5.8	0.0006-0.005-0.01	6.0±0.3
Altos los chilenos	PE-22	N31°E/60°	11.8	0.003-0.03-0.1	6.3±0.3
Cerro Morrito	PE-23	N63°E/60°	5.6	0.003-0.02-0.1	5.9±0.3
Pampa Trapiche	PE-24	N85°W/45°	18.5	0.001-0.01-0.1	6.5±0.3
Toquepala	PE-25	N62°W/90°	114	0.07-0.4-1.0	7.5±0.3
Micalaco	PE-26	N66°W/90°	32.6	0.001-0.01-0.1	6.8±0.3
Pampa Purgatorio	PE-27	N77°W/75°	27.9	0.05-0.12-1.0	6.8±0.3
Villacollo Norte	PE-28a	N75°W/45°	8.7	0.001-0.01-0.1	6.2±0.3
Villacollo Sur	PE-28b	N83°E/90°	21.8	0.001-0.01-0.1	6.6±0.3
Cerro Rocoso	PE-29	N31°E/70°	11.8	0.001-0.016-0.1	6.3±0.3
Cerro Caquilluco	PE-30	N71°W/90°	19.1	0.001-0.01-0.1	6.6±0.3
San Fracisco	PE-31	N44°W/60°	18.6	0.001-0.01-0.1	6.6±0.3

Table II lists the faults considered in the model, along with their seismic characteristics, including fault type, direction, dip, rupture length, most recent displacement time, estimated slip rate, and magnitude. The maximum magnitude for each fault was derived from the highest value among the Wells and Coppersmith [43], Anderson et al. [44], and Anderson et al. [45] relationships.

4. PROBABILISTIC SEISMIC HAZARD ANALYSIS

4.1. Soil Classification

For the calculation of ground shaking and uniform hazard spectra in Arequipa, the soil is classified as Type B, corresponding to Site Class B or rock, with an average shear-wave velocity in the upper 30 m (Vs_{30}) between 760 m/s and 1500 m/s, as specified in ASCE7-16. In line with the Peruvian standard E.030 of the National Building Code, this profile aligns with Type S1, covering Vs_{30} values from 500 m/s to 1500 m/s. The Vs_{30} value used for soil motion prediction is 760 m/s.

4.2. Ground Motion Models

Arango et al. [46] investigated the applicability of GMMs for subduction zones in Peru, Chile, and Central America, differentiating between interface and intraslab events. The study evaluated nine GMMs and assessed their performance using the maximum likelihood method proposed by Scherbaum et al. [47], which statistically analyzes the residuals between predicted and observed ground motions. Based on this evaluation, the authors recommended the use of Youngs et al. [48], Zhao et al. [49], and BC Hydro [50] for interface events, and BC Hydro [51] and Zhao et al. [49] for intraslab events.

In a separate study, Aguilar & Tarazona [3] applied the model selection methodology of Scherbaum, Delavaud, and Riggelsen [52] to assess the compatibility of subduction zone seismicity in the region. His findings suggest that the observed ground motions are best represented by the GMMs of Abrahamson et al. [51], Montalva [53], and Parker et al. [54], recommending their use for both interface and intraslab events.

4.3. Uncertainties

To account for epistemic uncertainties and reduce variability in the seismic hazard assessment, a logic tree approach was adopted using multiple GMMs with assigned weights. For subduction sources (both interface and intraslab), a set of five GMMs was employed: Abrahamson et al. [51], Montalva et al. [53], Youngs et al. [48], Zhao et al. [49], and Parker et al. [54], each assigned an equal weight of 0.20. In addition, to incorporating epistemic uncertainty in median ground motion predictions, the model of Abrahamson et al. [51] was considered with three branches representing the upper, central, and lower estimates of the median, with corresponding weights of 0.32, 0.36, and 0.32, respectively.

For crustal seismic sources, three GMMs were included with equal weighting: Boore et al. [55],

Campbell and Bozorgnia [56], and Chiou and Youngs [57]. This balanced weighting reflects the absence of a clear preference among these models and supports a robust characterization of ground motion variability in shallow crustal environments.

Additionally, two declustering methodologies were applied to the seismic catalog to assess sensitivity to temporal and spatial clustering of events: the window-based method of Gardner and Knopoff [25], and the stochastic declustering approach proposed by van Stiphout et al. [21]. Variations in the β parameter and seismic activity rates are also considered. To address variability-related uncertainties, a range of maximum magnitudes and recurrence rates for crustal faults, tied to differing slip rates, is incorporated (see **Table II**). These model variations are synthesized using a logic tree which combines the results of different scenarios and decisions with their respective weights, integrating both epistemic and variability uncertainties (see **Fig. 5**).

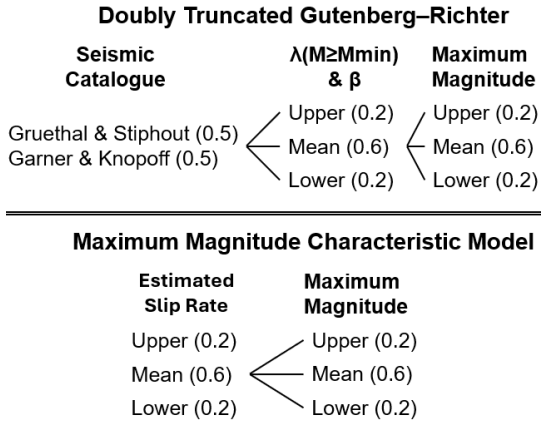

Fig. 5. Logic Tree Framework for PSHA

In this probabilistic seismic hazard analysis, uncertainties associated with seismic source characterization were rigorously incorporated using a logic tree approach. For the seismic sources modeled with a truncated exponential model, a declustering method was applied with a value of 0.5 for the Gruenthal and Stiphout method, and similarly, 0.5 for the Garner and Knopoff method. For the truncated exponential model parameters, the mean values of λ(M≥Mmin) and β were set to 0.6, with the upper and lower bounds of a and b assigned values of 0.2 each. The maximum magnitude was modeled with a weight distribution of 0.2 for the upper bound, 0.6 for the mean, and 0.2 for the lower bound. Fault sources, represented with the Maximum Magnitude Model, were assigned a weight of 0.2 for the lower slip rate, 0.6 for the mean, and 0.2 for the upper slip rate. The maximum magnitude for faults was similarly characterized with a weight distribution of 0.2 for the upper bound, 0.6 for the mean, and 0.2 for the lower bound, ensuring a comprehensive representation of uncertainties in both the seismic source and fault modeling .

5. RESULTS

The probabilistic seismic hazard analysis was conducted using the open-source software R-Crisis (v20.0), following the methodology outlined in by Ordaz & Salgado-Gálvez [58]. **Fig. 6** presents the peak ground acceleration for a 10% probability of exceedance in 50 years in Arequipa city. In the northeastern districts—Cayma, Selva Alegre, Mariano Melgar, and Paucarpata—the acceleration ranges from 0.435 to 0.440g. In the central areas, including Yanahuara, Socabaya, Characato, and José Luis Bustamante districts, it increases to 0.445–0.450g. The districts of Sachaca and Hunter exhibit accelerations between 0.450 and 0.455g, while in the southwestern districts, such as Uchumayo and Tiabaya, the acceleration peaks at 0.460g.

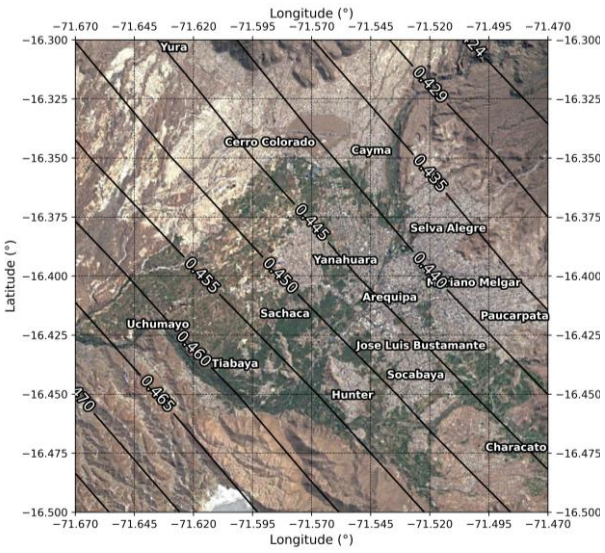

Fig. 6. Peak Ground Acceleration (g) in Arequipa City – 10% Probability of Exceedance in 50 Years – 475 Years Return Period

Fig. 7 depicts the peak ground acceleration for a 2% probability of exceedance over 2475 years in Arequipa. In the northeastern districts, including Cayma, Selva Alegre, Mariano Melgar, and Paucarpata, the acceleration is 0.805g. In the city center and surrounding districts such as Yanahuara, Socabaya, Characato, and José Luis Bustamante, the value rises to 0.820g. In Sachaca and Hunter, the acceleration reaches 0.836g. while in the southwestern districts of Uchumayo and Tiabaya, it peaks at 0.851g. **Fig. 8** presents the Uniform Hazard Curves for various probabilities of exceedance in 50 years at the center of Arequipa City.

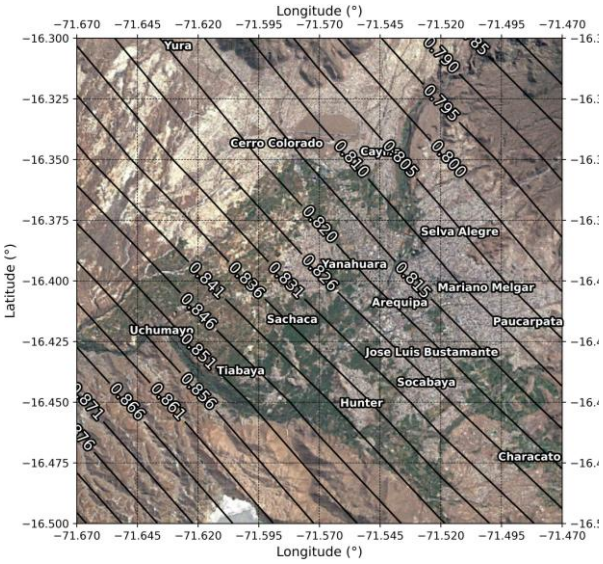

Fig. 7. Peak Ground Acceleration (g) in Arequipa City – 2% Probability of Exceedance in 50 Years – 2475 Years Return Period

To understand how different parameters associated with seismic hazard influence the model, seismic disaggregation is performed. This process evaluates the impact of various seismic sources on the total hazard, considering magnitude, distance to the source, and epsilon, which measures the deviation of ground motion from the predicted mean value. The intensity of ground motion depends on the magnitude (M) and distance (R) to the causative event, although there is significant variability in empirical records for the same M and R. Seismic disaggregation was conducted for 0.5%, 1%, 2%, 5%, and 10% of probability of exceedance in 50 years, considering PGA, 0.15s, and 1s acceleration periods with 5% damping spectra. The results of the seismic disaggregation indicate that, for PGA and the periods of 0.15s and 1s, the primary contributor to seismic hazard in the city of Arequipa is the intraslab source F5. This source is characterized by earthquakes in the range of M 7.5 to 8 and a distance between 100 and 150 km.

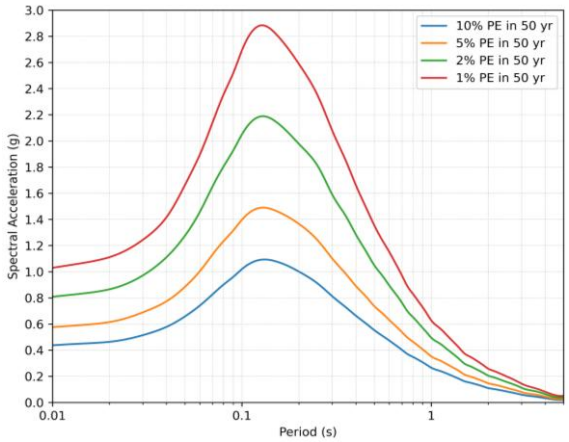

Fig. 8. Uniform Hazard Spectra at the Center of Arequipa City – 5% damping – Soil Class B (Vs_{30}=760 m/2)

Fig. 9 illustrates the probability of exceedance (PE) for various seismic sources as a function of spectral acceleration (Sa) at a period of approximately 0 seconds (T ≈ 0 s), which corresponds to Peak Ground Acceleration (PGA), providing insight into the relative contribution of each source to the seismic hazard at the site. The y-axis represents the probability of exceedance, the standard metric used in seismic hazard curves, while the x-axis denotes PGA. Each hazard curve corresponds to a different seismic source zone and shows its individual contribution to the hazard. The left subfigure presents the hazard curves for 10 area-type sources—including crustal, interface, and intraslab zones—modeled using the doubly truncated Gutenberg–Richter recurrence model. The right subfigure displays the hazard curves for Quaternary faults, modeled using a characteristic earthquake approach based on their maximum expected magnitudes. The legend identifies each seismic source, and the curves enable a direct comparison of their relative impact. Horizontal red lines indicate constant exceedance probabilities corresponding to standard return periods (e.g., 10% in 50 years ≈ 475-year return period), serving as reference thresholds for interpreting the curves. The results indicate that the intermediate intraslab source F5 is the dominant contributor to seismic hazard, followed by the interface source F2. In contrast, the deep intraslab source F9 has the least influence among the subduction-related sources. Among the crustal sources, the area-type source F10 is the most significant, with events ranging from M 4.5 to M 7.5 governed by the truncated Gutenberg–Richter model. Other crustal sources were modeled using the characteristic approach to capture their maximum magnitude potential. Following F10, the Solarpampa and Trigal faults in Arequipa, along with the Toquepala fault in Tacna, are the next most relevant contributors; however, their influence is only apparent at low exceedance probabilities, specifically below 2% in 50 years.

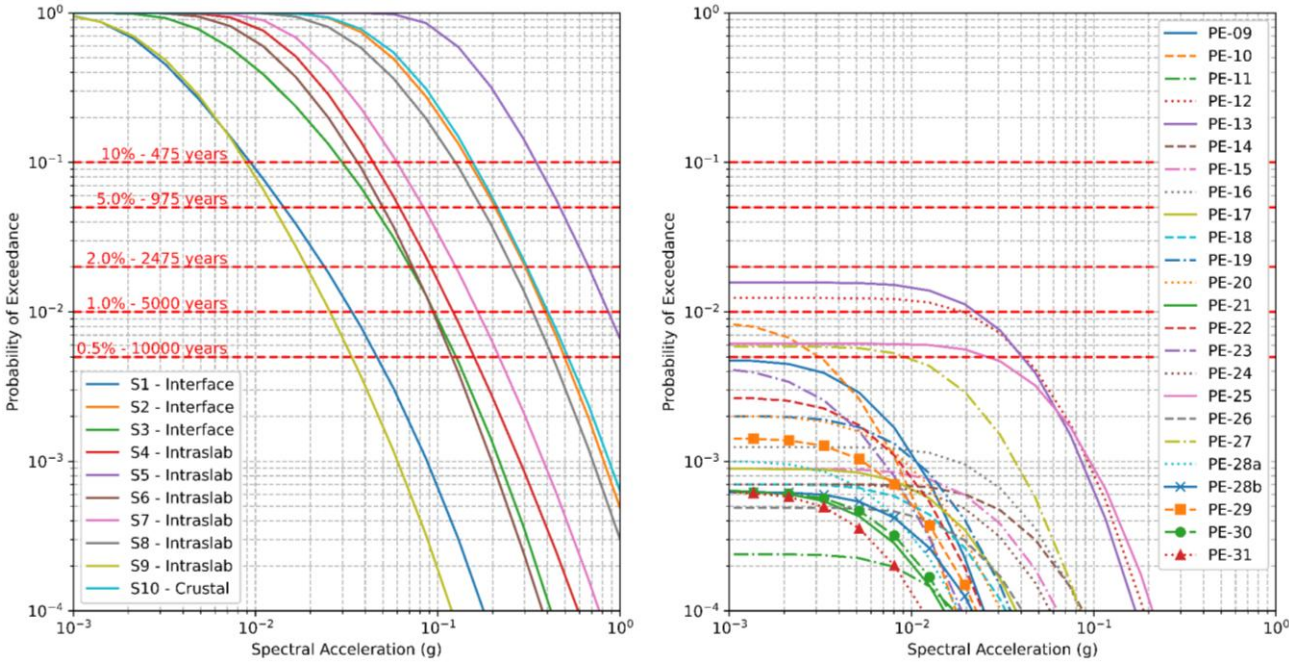

Fig. 9. Probability of Exceedance for All Seismic Faults Using (a) Truncated Exponential Model and (b) Maximum Magnitude Model. Horizontal lines indicate constant probabilities of exceedance, corresponding to standard return periods (e.g., 10% in 50 years ≈ 475 years)

CONCLUSIONS

- The probabilistic seismic hazard analysis for downtown Arequipa, conducted on Type B soil (Vs_{30} = 760 m/s), yielded ground acceleration values for different probabilities of exceedance in 50 years. For a 10% probability of exceedance, the PGA is 0.44 g, with spectral accelerations of 1.08 g at T = 0.15 s and 0.27 g at T = 1.0 s. These values increase to 0.58 g, 1.47 g, and 0.35 g, respectively, for a 5% probability of exceedance, and to 0.80 g, 2.15 g, and 0.49 g for a 2% probability of exceedance. The PGA results for 10% and 2% probabilities of exceedance in 50 years align closely with those of Medina et al. [59], who reported 0.45 g and 0.80 g, and Aguilar & Tarazona [3], who found 0.4 g and 0.72 g, respectively.
- Seismic disaggregation indicates that earthquakes with magnitudes in the range of M 7.5 to 8 and distances between 100 and 150 km contribute most significantly to seismic hazard for PGA, S exccedancea(0.15), and Sa(1.0). The intermediate intraslab source F7, followed by the interface source F2, are the primary contributors to seismic hazard. This finding is consistent with the study by Monroy et al. [1], which also indicates that the intermediate source S7 contributes most to seismic hazard with magnitudes of 7.5 to 8.0 at distances of 125 to 150 km.
- Crustal faults, due to their low slip rates and consequently high recurrence intervals, contribute minimally to seismic hazard when considering a maximum magnitude model. The faults with the least impact on seismic hazard include the San Francisco Fault in Tacna and the Vilcanota Fault in Cuzco. For the PSHA, the Solarpampa, Trigal, Toquepala, Pampa de Purgatorio, and Ocongate faults contribute to seismic hazard only at very low probabilities of exceedance, specifically below 2% in 50 years. Other faults show no contribution to seismic hazard, even at exceedance probabilities as low as 0.5% in 50 years.

ACKNOWLEDGMENTS

This research was conducted as part of my journey to obtain a master's degree in Geotechnical Engineering at the University of Engineering in Lima, Peru.

REFERENCES

[1] M. Monroy, A. Hull, M. Martinez, & A. Bolanos, Estimation of Parameters for Seismic Design in Peru. 5th International Conference on Earthquake Geotechnical Engineering. Santiago, Chile, 2011

[2] R. Youngs, & K. Coppersmith, Implication of fault slip rates and earthquake recurrence models to probablistic seismic hazard estimatesv. *Bulletin of the Seismological Society of America*, Vol 75, No. 4, pp. 939-964, 1985, doi: 10.1785/BSSA0750040939

[3] Z. Aguilar, & J. Tarazona, New Seismicity Based Seismic Sources and Hazard Model for Peru. 18th World Conferece on Earthquake Engineering, 2024

[4] I. Muldashev, & S. Sobolev, What controls maximum magnitudes of giant subduction earthquakes. Geochemistry, Geophysics, Geosystems, 21, e2020GC009145, 2020, doi: 10.1029/2020GC009145.

[5] S. Carena, Subduction-plate topography and nucleation of great and giant earthquakes along the south american trench. *Seismological Resarch Letters*, Vol 82, No. 5, 2011, doi: 10.1785/gssr.82.5.629

[6] J. Tarazona, Z. Aguilar, N. Pulido, , C. Gonzales, , F. Lazares, Seismicity based maximum magnitude estimation of subduction

earthquakes in Peru. Journal of Disaster Research, vol. 18 No.4, 2023, doi: 10.20965/jdr.2023.p0308
[7] E. Silgado, Historia de los sismos más notables ocurridos en el Peru (1513-1974), Instituto de Geologia y Mineria, Boletin No. 3, Serie C, Geodinamica e Ingenieria, Lima – Peru, 1978
[8] A. Dorbath, A. Cisternas, & C. Dorbath, Assessment of the size of large and great historical earthquakes in Peru. Bulletin of the Seismological Society of America, Vol. 80, No. 3, 551-576, 1990, doi: 10.1785/BSSA0800030551
[9] H. Tavera, C. Agüero, E. Fernández, & S. Rodríguez, Catálogo sísmico del Perú 1471-1982. Instituto Geofisico del Peru Direccion de Sismologia, 2001. [Online]. Available: http://hdl.handle.net/20.500.12816/789
[10] H. Tavera, C. Aguero, & E. Fernandez, Catalogo general de isosistas para sismos peruanos. Instituto Geofisico del Peru, Lima – Peru, 2016. [Online]. Available: http://hdl.handle.net/20.500.12816/791
[11] IGP, Instituto Geofisico del Peru, Sismos Instrumentales, 2024, [Online]. Available: https://ultimosismo.igp.gob.pe/descargar-datos-sismicos
[12] USGS, United States Geological Survey, Earthquake Catalog. [Online]. Available: https://earthquake.usgs.gov/earthquakes/search
[13] ISC, International Seismological Centre, Eartuquake Catalog. [Online]. Available: https://doi.org/10.31905/D808B830
[14] CMT, Global Centroid-Moment-Tensor, Earthquake Catalog. [Online]. Available: https://www.globalcmt.org/CMTsearch.html
[15] NEI, National Earthquake Information Center, Earthquake Catalog. [Online]. Available: https://www.usgs.gov/programs/earthquake-hazards/national-earthquake-information-center-neic
[16] National Geophysical Data Center / World Data Service (NGDC/WDS), NCEI/WDS Global Significant Earthquake Database, NOAA National Centers for Environmental Information, 2024, doi: 10.7289/V5TD9V7K
[17] R. McGuire, Seismic Hazard and Risk Analysis, Earthquake Engineering Research Institute, 2004
[18] T. Hanks, & H. Kanamori, A moment magnitude scale. Journal of Geophysical Research, Vol. 84, 2348-2350, 1979, doi: 10.1029/JB084iB05p02348
[19] F. Kadirioğlu, & R. Kartal, The new empirical magnitude conversion relations using an improved earthquake catalogue for Turkey and its near vicinity (1900-2012). TURKISH JOURNAL OF EARTH SCIENCES, Vol. 25. 300-310, 2016, doi: 10.3906/yer-1511-7
[20] E. Scordilis, Empirical Global Relations Converting Ms and mb to Moment Magnitude, Journal of Seismology, 225-236, 2006, doi: 10.1007/s10950-006-9012-4
[21] T. van Stiphout, , J. Zhuang, and D. Marsan, Seismicity declustering, Community Online Resource for Statistical Seismicity Analysis, 2012, doi:10.5078/corssa-52382934
[22] L. Knopoff, and J. Gardner, Higher Seismic Activity During Local Night on the Raw Worldwide Earthquake Catalogue, Geophys. J. R. astr. Soc., 28, 311-313, 1972, doi: 10.1111/j.1365-246X.1972.tb06133.x
[23] K. Maeda, The use of foreshocks in probabilistic prediction along the Japan and Kuril Trenches, Bulletin of the Seismological Society of America, 86, 242-254, 1996, doi: 10.1785/BSSA08601A0242
[24] R. Uhrhammer, Characteristics of Northern and Central California Seismicity, Earthquake Notes, Vol. 57, No. 1, pp. 21, 1986
[25] J. K. Gardner, and L. Knopo, Is the sequence of earthquakes in Southern California, with aftershocks removed, Poissonian?, Bull. Seis. Soc. Am., Vol. 64, No. 5, 1363-1367, 1974, doi: 10.1785/BSSA0640051363
[26] J. Stepp, Analysis of Completeness of the Earthquake Sample in the Puget Sound Area and its Effect on Statistical Estimates of Earthquake Hazard. National Oceanic and Atmospheric Administration Environmental Research Laboratories Boulder, Colorado, 1972
[27] M. Cisternas, M. Carvajal, R. Wesson, L.L. Ely, and N. Gorigoita, Exploring the Historical Earthquakes Preceding Giant 1960 Chile Earthquake in a Time-Dependent Seismogenic Zone, Bulletin of the Seismological Society of America, 2017, doi: 10.1785/0120170103.
[28] M. K. Giovanni, S. L. Beck, and L. Wagner, The June 23, 2001 Peru Earthquake and the Southern Peru Subduction Zone. Geophysical Research Letters, Vol. 29, No 21, 2018, doi: 10.1029/2002GL015774.
[29] M. Pasyanos, T. Guy Masters, G. Laske, & Z. Ma, LITHO1.0: An updated crust and lithospheric model of the Earth. Journal of Geophysical Research: Solid Earth, Vol. 119, No. 3, p. 2153 -2173, 2014, doi: 10.1002/2013JB010626
[30] M. Pagani, K. Johnson, & J. Garcia Palaez, Modelling subduction sources for probabilistic seismic hazard analysis. Geological Society of London, Special Publication, 501, 225-244, 2020, doi: 10.1144/SP501-2019-120
[31] B. Gutenberg, and C.F. Richter, Frequency of Earthquakes in California. Bulletin of the Seismological Society of America, 34, 185-188, 1944, doi: 10.1785/BSSA0340040185
[32] C.A. Cornell, and E. Vanmarcke, The Major Influences on Seismic Risk. Proceedings of the IV World Congress in Earthquake Engineering, Santiago, 13-18 January 1969, 169-183
[33] M. W. Herman, & R. Govers, Locating fully locked asperities along the South America subduction megathrust: A new physical interseismic inversion approach in a Bayesian framework, Geochemistry, Geophysics, Geosystems, 21, e2020GC009063, 2020, doi: 10.1029/2020GC009063
[34] G. Hayes, G. Moore, D. Portner, M. Hearne, H. Flamme, M. Furtney's, & G. Smoczyk, Slab2, a comprehensive subduction zone geometry model. Science, Vol.362, No.6410, pp. 58-61, 2018, doi: 10.1126/science.aat4723
[35] D. H. Weichert, Estimation of the earthquake recurrence parameters for unequal observation periods for different magnitudes, Bull. Seismol. Soc. Am. Vol. 70, no. 4, pp. 1337-1346, 1980, doi: 10.1785/BSSA0700041337
[36] I. Muldashev, & S. Sobolev, What controls maximum magnitudes of giant subduction earthquakes, Geochemistry, Geophysics, Geosystems, 21, e2020GC009145, 2020, doi: 10.1029/2020GC009145
[37] S. Carena, Subduction-plate topography and nucleation of great and giant earthquakes along the south american trench, Seismological Resarch Letters, Vol 82, No. 5. 2011, doi: 10.1785/gssr.82.5.629
[38] J. Tarazona, Z. Aguilar, N. Pulido, C. Gonzales, F. Lazares, H. Miyake, Seismicity based maximum magnitude estimation of subduction earthquakes in Peru, Journal of Disaster Research, vol. 18 No.4, 2023, doi: 10.20965/jdr.2023.p0308
[39] A. Kijko, Estimation of the maximum earthquake magnitude, mmax, Pure appl. geophys. 161, 1655-1681. 2004, doi: 10.1007/s00024-004-2531-4
[40] E. Kausel, & J. Campos, The Ms=8 tensional earthquake of 9 December 1950 of northen Chile and its relation to the seismic potential of the region. Physics of the Earth and Planetary Interiors, Vol 72, 220 - 235, 1992, doi: 10.1016/0031-9201(92)90203-8
[41] C. Benavente, G. Delgado, B. Garcia, E. Aguirre, & L. Audin, Neotectonica, evolución del relieve y peligro sismico en la region arequipa. INGEMMET, Boletin Serie C: Geodinamica e Ingenieria Geologica N64, 2017
[42] J. Machare, C. Fentona, M. Machette, A. Lavenu, C. Costa, & R. Dart, Database and map of quaternary faults and folds in Peru and its offshore region. U.S. Geological Survey Open-File Report 03-451, 55p, 2003, doi: 10.3133/ofr03451
[43] D. Wells, & K. Coppersmith, New empirical relationships among magnitude, rupture, length, rupture width, rupture area, and surface displacement, Bulletin of the Seismological Society of America, 84, No. 4, 974-1002, 1994, doi: 10.1785/BSSA0840040974
[44] J. Anderson, S. Wesnousky, & M. Stirling, Earthquake Size as a Function of Fault Slip Rate. Bulletin of the Seismological Society of America, Vol. 86, No 3, pp. 683-690, 1996, doi: 10.1785/BSSA0860030683
[45] J. Anderson, G. Biasi, & S. Wesnousky, Earthquake Magnitude Estimation from Fault Dimensions and Slip Rate, Final Technical Report, 2016, Nevada Seismological Laboratory, University of Nevada.
[46] M. Arango, F. Strasser, J. Bommer, J. Cepeda, R. Boroschek, D. Hernandez, & H. Tavera, An evaluation of the applicability of current ground-motion models to the south and central america

subduction zones, Bulletin of the Seismological Society of America, Vol. 102, No 1, pp. 143-168, 2012, doi: 10.1785/0120110078
[47] F. Scherbaum, F. Cotton, & P. Smit, On the use of response spectral-reference data for the selection and ranking of ground-motion models for seismic-hazard analysis in regions of moderate seismicity: The case of rock motion, Bulletin of the Seismological Society of America, 94, 2164-218, 2004, doi: 10.1785/0120030147
[48] R. R. Youngs, S. -J. Chiou, W. J. Silva and J. R. Humphrey, Strong Ground Motion Attenuation Relationships for Subduction Zone Earthquakes, Seismological Research Letters, Vol. 68, No. 1, 58-73, 1997, doi: 10.1785/gssrl.68.1.58
[49] J. Zhao, J. Zhang, A. Asano, Y. Ohno, T. Oouchi, Y. Takahashi, Y. Fukushima, Attenuation relations of strong ground motion in Japan using site classification based on predominant period. Bulletin of the Seismological Society of America, 96, 898-913, 2006, doi: 10.1785/0120050122
[50] BC Hydro, PSHA for Western Canada: Volume 3-Ground Motion Models. BC Hydro Report E658, July 2010, BC Hydro, Vancouver, Canada
[51] N. G. Norman Abrahamson, BC Hydro Ground Motion Prediction Equations For Subduction Earthquakes. Earthquake Spectra, 2016, doi: 10.1193/051712EQS188MR
[52] F. Scherbaum, E. Delavaud, C. Riggelsen, Model Selection in Seismic Hazard Analysis: An Information-Theoretic Perspective, Bulletin of the Seismological Society of America, Vol 99, No. 6, 3234-3247, 2009, doi: 10.1785/0120080347.
[53] B. R.-M. Montalva et al, Ground-Motion Prediction Equation for the Chilean Subduction Zone. Bulletin of the Seismological Society of America, 901-911, 2017, doi: 10.1785/0120160221
[54] G. Parker, J. Stewart, D. Boore, G. Atkinson, & B. Hassani, NGA-Subduction Global Ground-Motion Models with Regional Adjustment Factors. Pacific Earthquake Engineering Research Center, 2020, Headquarters at the University of California, Berkeley.
[55] D. Boore, J. Stewart, E. Seyhan, & G. Atkinson, NGA-West2 Equations for predicting PGA, PGV, and 5% damped PSA for shallow crustal earthquakes. Earthquake Spectra, Volume 30, No. 3, pages 1057-1085, 2014, doi: 10.1193/070113EQS184M
[56] K. Campbell, Y. Bozorgnia, NGA-West2 Ground motion model for the average horizontal components of PGA, PGV and 5% damped linear acceleration response spectra. Earthquake Spectra, Volume 30, No. 3, pp. 1087-1115, 2014, doi: 10.1193/062913EQS175M
[57] B.-J. Chiou, & R. Youngs, Update of the Chiou and Youngs NGA model for the average horizontal component of peak ground motion and response spectra. Earthquake Spectra, Volume 30, No. 3, pp. 1117-1153, 2014, doi: 10.1193/072813EQS219M
[58] M. Ordaz, & M.A. Salgado-Galvez. R-Crisis v20 Validation and Verification Document. ERN Technical Report. Mexico City, Mexico, 2020
[59] F. Medina, S. Harmsen, & S. Barrientos, Probabilistic Seismic Hazard Analysis for Chile. 16th World Conference on Earthquake Engineering, 2017, January